Check for updates

Solar-pumped fiber laser using a solid-state luminescent solar collector

MASAMORI ENDO,[1,*] **KOHEI YAMAMOTO,**[1] **STEPHAN DOTTERMUSCH,**[2] **IAN A. HOWARD,**[2] **BRYCE S. RICHARDS,**[2] **RYOTA TOMIZAWA,**[3] **AND TAIZO MASUDA**[3,4]

[1] *Department of Physics, Tokai University, 4-1-1 Kitakaname, Hiratsuka, 259-1292, Japan*
[2] *Institute of Microstructure Technology, Karlsruhe Institute of Technology, 76344 Eggenstein-Leopoldshafen, Germany*
[3] *Carbon Neutral Development Division, Toyota Motor Corporation, 1200 Mishuku, Susono, Shizuoka, 410-1193, Japan*
[4] *Institute for Advanced Science, The University of Electro-Communications, 1-5-1 Chofugaoka, Chofu, Tokyo, 182-8585, Japan*
*endo@tokai.ac.jp

Abstract: We have developed a fully planar solar-pumped fiber laser using a solid-state luminescent solar collector (LSC). This laser does not use any focusing device, such as a lens or mirror; thus, it can lase without tracking the sun. Our developed device with an aperture of 30 cm emits 15 mW, corresponding to an optical-to-optical conversion efficiency of 0.023% and a collection efficiency of 0.21 W/m². A 12-fold improvement over a previously developed liquid LSC is achieved by combining the total internal reflection of the solid-state LSC with dielectric multilayer mirrors. The observed laser power is in good agreement with that predicted via numerical simulation, demonstrating the effectiveness of our proposed method.

1. Introduction

Solar pumped lasers (SPLs) are optically pumped lasers that use natural sunlight as a pump source. Oscillation through various media, including gas, liquid and solid media, has been reported thus far, but the current mainstream research is on solid-state lasers using the trivalent neodymium ion (Nd^{3+}) as the laser medium due to its high optical-to-optical conversion efficiency [1–7].

Potential applications of SPLs are expected in the energy field. For example, the conversion of sunlight into coherent laser light can generate high temperatures beyond the thermodynamic limit, and a Mg/MgO energy storage concept has been proposed [8]. Since the thermal relaxation loss is minimal for monochromatic light with wavelengths close to the bandgap of a silicon photovoltaic device, a highly efficient optical wireless power transmission (OWPT) based on the solar-pumped fiber laser has been proposed [9,10]. In addition, laser light can be converted to ultraviolet (UV) light via nonlinear crystals; thus, the combination of SPL with photocatalytic water splitting, which is efficient in UV [11,12], can enhance its overall efficiency of hydrogen production. The very simple structure of the SPL, which in principle has neither active electronics nor moving parts, has advantages over other lasers, especially in space. There are numerous proposed extraterrestrial applications, such as propulsion [13], power transmission [14,15] and communication [16,17].

The challenge with conventional SPLs is that the pump light source, sunlight, is incoherent white light that requires tight focusing to achieve sufficient population inversion in the laser medium. For this reason, all SPLs published to date have relied on a primary concentrator comprised of a large lens or mirror [18]. In turn, this requires precise tracking of the sun to

maintain illumination of the laser medium [19]. These issues are notable obstacles to the practical application of SPLs.

To address this fundamental problem of SPLs, we have proposed an SPL without condenser optics. The schematic of the "fully planar solar-pumped fiber laser (SPFL)" is shown in Fig. 1. The basic principle of this laser is described as follows: An Nd^{3+}-doped active optical fiber is contained in a thin, bowl-shaped housing, which is made entirely of highly reflective mirrors (HRM). In addition, the surface facing the sun is a dichroic mirror (DM) that transmits shorter wavelengths and reflects longer wavelengths. The housing is filled with a liquid sensitizer in which the fiber is immersed. Sunlight transmitted through the dichroic mirror is absorbed by the sensitizer and fluoresces at wavelengths longer than the absorbed wavelength. Because the cutoff of the dichroic mirror is set shorter than the wavelength of the fluorophore, fluorescence cannot exit the housing and travels back and forth within the housing until it is absorbed by the fiber. The active fiber then generates gain, and the laser oscillates.
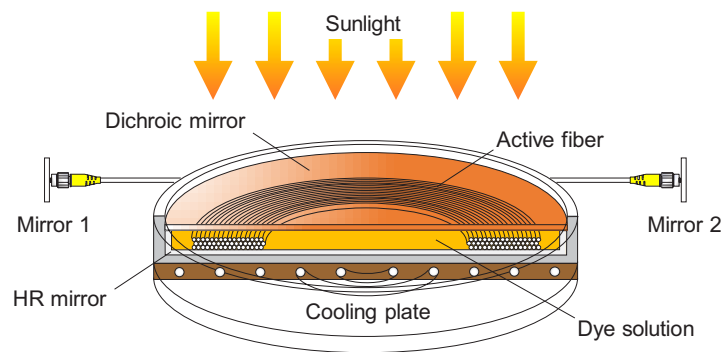
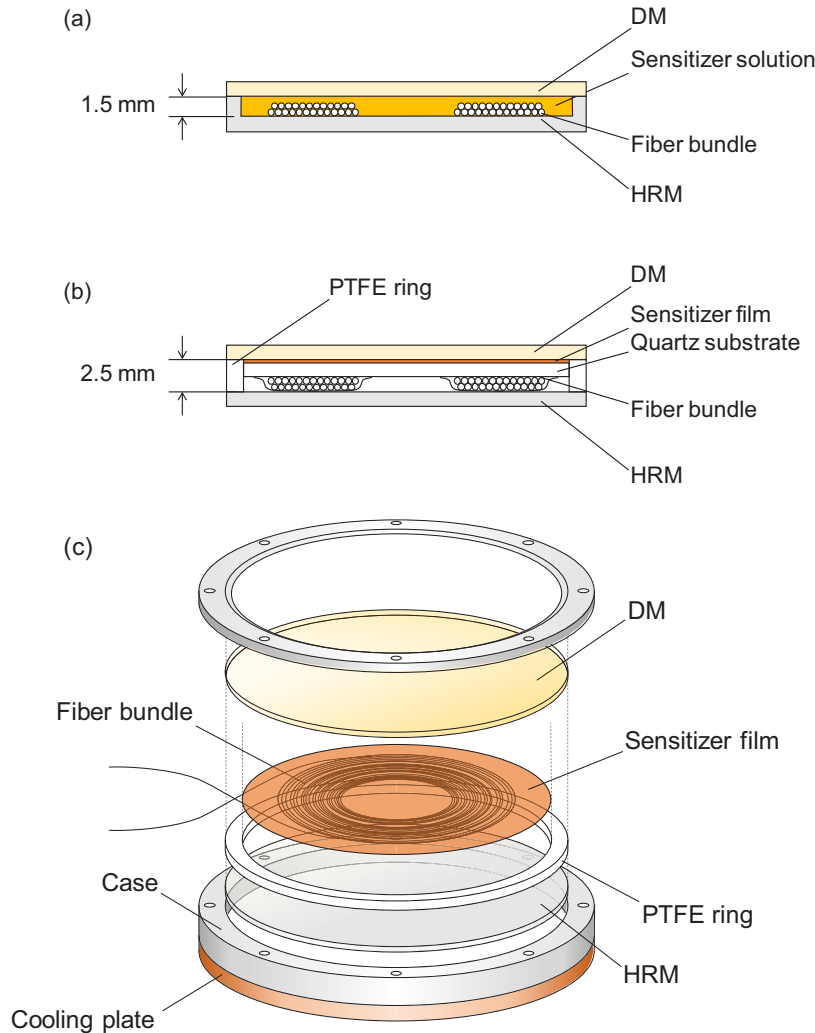**Fig. 1.** Schematic drawing of a fully planar SPFL

Based on this principle, we previously fabricated a device with a diameter of 30 cm [20]. Initial studies showed that the population density of the lower laser level ($^4I_{11/2}$) of Nd^{3+} ions at room temperature interfered with the positive gain generation [21]; thus, the entire device was cooled below −30°C by conductive cooling. Furthermore, the simulation calculations showed that the maximum output power was achieved at a fiber length of 10 km for a 30 cm diameter device [22]; however, the fiber length was limited to 190 m due to budget constraints. Therefore, this experimental device was a proof-of-principle device. As a result of the above experiments, a maximum laser power of 1.3 mW was obtained [20]. Since the sunlight power density at the Earth's surface is 1 kW/m^2, the incident power can be calculated to be 70 W; thus, the optical-to-optical conversion efficiency is only 2×10^{-5}. To our knowledge, this is the first time that an SPL has been successfully oscillated without a "hard" focusing device, such as a lens or a mirror.

2. Methods

2.1. Current challenges of the fully planar SPL

The main reason for the low optical-to-optical conversion efficiency is the short fiber, as mentioned above; however, there are two additional issues that need to be addressed. One is the use of an organic dye (Rhodamine 6 G) that fluoresces orange as a sensitizer such that the cutoff of the dichroic mirror is set at 570 nm [20], removing a significant portion of the spectral components of sunlight. The other issue is that the top layer of the dielectric multilayer coating of the DM and HRM needs to be in contact with a liquid that has a refractive index closer to that of the dielectric; thus, in principle, high reflectivity cannot be achieved, and photon confinement is impeded.

To address the first problem, we plan to use and develop perovskite quantum dots as sensitizers instead of organic dyes. We have already demonstrated the tunability of the fluorescence wavelength in preliminary experiments, and laser oscillation was accomplished under 50× sunlight with a primary concentrator [23]. To address the second problem, we then propose the use of solid-state LSCs [24,25]. Figure 2(a) and (b) shows a cross section of a fully planar SPFL with a conventional configuration and using a solid-state LSC, respectively. To aid the reader's understanding, Fig. 2(c) shows the components of the new SPFL disassembled and viewed from an angle.

Fig. 2. (a) Cross-sectional view of a fully planar SPFL using a liquid LSC (conventional). (b) Cross-sectional view of a fully planar SPFL using a solid-state LSC (proposed). (c) Structural drawing of the new SPFL.

In the conventional configuration, the active fiber is immersed in a liquid; conversely, in our proposed system, the fiber is attached to a quartz substrate with an optical adhesive. On the opposite side, the LSC is coated with a fluorinated polyurethane film impregnated with a sensitizer. The DM/HRM is the same as in the liquid LSC; however, its confinement efficiency is dramatically improved when the top layer of the dielectric multilayer is in contact with air.

Although efficient light confinement is expected from total internal reflection (TIR) between the LSC and air [26], previous research has shown that DM/HR is a necessary component, with 40% of all photons confined by TIR, while the remaining 60% are confined by DH/HRM [25].

2.2. Configuration of the solid-state LSC

The solid-state LSC fabricated in this study consisted of a 30 cm diameter, 1.0 mm thick fused quartz plate, with the coiled fiber attached to it using InvisiSil OP1012 optical adhesive (Momentive), and a thin film sensitizer layer. The optical fiber was the same as that used in previous studies (Furukawa Electric) [20,21], with a core diameter of 16 μm and a Nd^{3+} concentration of 0.5 at%. Before attaching the fiber to the substrate, the protective resin layer was removed, leaving the 125 μm diameter cladding exposed.

The sensitizer film was applied to the substrate as follows. The fluorinated polyurethane host was prepared using the polyol Lumiflon (AGC Chemicals) and isocyanate Duranate (Asahi Kasei). The two components were mixed (NCO/OH = 1) by magnetic stirring. Then, Lumogen F Orange 240 and Yellow 083 (BASF) dyes were dissolved in chloroform (FUJIFILM Waco Pure Chemical) and admixed to the host. The concentrations on the host were 0.39 mg/g (O240) and 0.79 mg/g (Y083). The compound was blade-coated on the substrate at a desired thickness (approx. 200 μm). After casting, the film is left in a dark, ventilated environment for the next 48 hours to allow the solvents to evaporate and the polyurethane to cure. The resulting film thickness was approximately 80 μm, and the optical density at 532 nm was 0.6. For further details of the dye film, refer to previous studies [24,25].

Figure 3 shows the absorption and emission spectra of the dye film. Their magnitudes are normalized to their peak values. The black plot is the reflectivity of the DM at normal incidence. The quantum yield of the dye film was measured using a 532 nm laser as the pump source. The measured value was $75 \pm 2\%$.
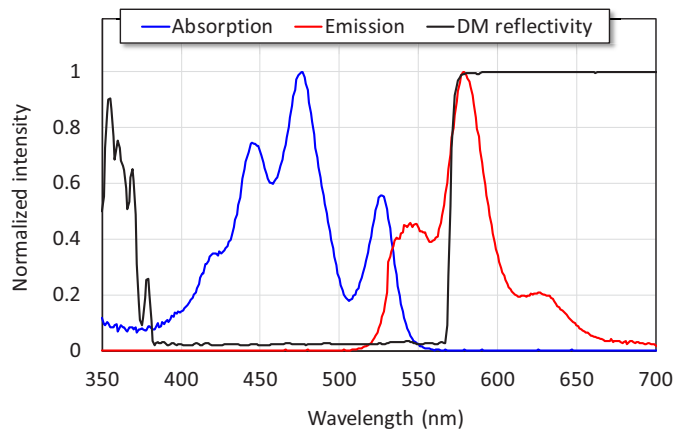
Fig. 3. Absorption and emission spectra of the dye film. The black line shows the DM reflectivity.

A polytetrafluoroethylene (PTFE) ring was placed on the side of the LSC and sandwiched between the DM and the HRM. The HRM of the liquid LSC had a bowl shape due to the need to keep it watertight, creating technical difficulties in applying a highly reflective dielectric layer on the sides. Since a previous study showed that a diffuse side reflector could achieve 90% of the performance of specular reflectors [25], a combination of a flat HRM and a PTFE ring was used; this also functioned as the support of the DM, providing the necessary clearance between the DM and HRM.

In this study, two disks were fabricated: one with a fiber length of 105 m and the other with a fiber length of 290 m. The disk with the shorter fiber length was a prototype to learn the technique for designing, fabricating, and conducting experiments with a solid-state LSC. A disk with approximately three times the fiber length was subsequently fabricated and tested outdoors, but a fiber inside the disk was accidentally broken before sufficient data could be obtained.

2.3. Experimental setup

In this study, small-signal gain measurements and laser oscillation experiments were performed on a fully planar SPFL with a solid-state LSC using natural sunlight as the pump source.

The gain measurement setup is shown in Fig. 4. A fiber-coupled superluminescent diode (SLD, Thorlabs SFC1050P) was injected into the active fiber at one end, and the emitted light was received at the other end by a fiber spectrometer (Ocean Optics NIRQuest). $A(\lambda)$ is the spectral intensity of the probe signal measured by the spectrometer with solar illumination, and $B(\lambda)$ is the spectral intensity without solar illumination. Since the spontaneous emission from the sunlight absorbed by the active fiber contributed a significant fraction of the measured intensity of $A(\lambda)$, we measured the spectral intensity of the spontaneous emission by turning off the SLD and illuminating the sunlight. $C(\lambda)$ is this spectral intensity. In this case, the following relationship is obtained:

$$G(\lambda) = \frac{A(\lambda) - C(\lambda)}{B(\lambda)}. \tag{1}$$

This relationship is the one-pass differential gain of the SPL; however, it is not the net gain because the attenuation of the probe light due to fiber loss is not considered. However, this expression is useful as a simple gain measurement method.
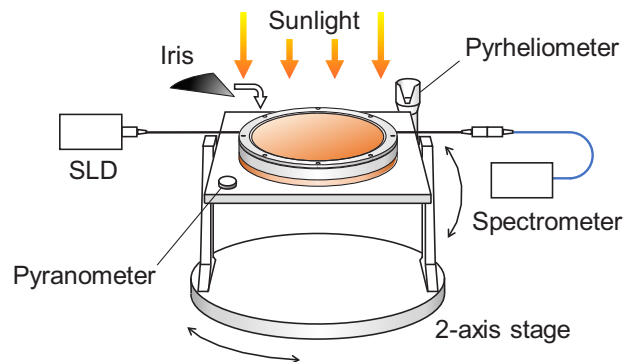
Fig. 4. Schematic drawing of the gain measurement setup.

The setup for the laser oscillation experiment is shown in Fig. 5. The optical resonator consisted of a highly reflective mirror M1 and a partially transmissive mirror M2; M1 was a dichroic mirror with transmission at 808 nm. The fiber was terminated with a ferrule connector (FC)-type fiber receptacle that contacted the mirror to form a pigtail resonator [27]. The advantages of pigtail resonators are that the transmittance of M2 can be changed easily, quickly, and nondestructively (without splicing the fiber). The scattering loss of the pigtail mirror was reported to be 0.07 dB [27], which was comparable to the splice loss of a single-mode fiber.

The loss in the pigtail mirror was sensitive to the distance between the fiber end and the mirror. Therefore, before performing solar pumping experiments, the laser was longitudinally pumped by an 808 nm laser diode (LD) from M1, and the relative positions of the mirror and connector were adjusted to minimize resonator loss. The LD was then turned off, sunlight was irradiated
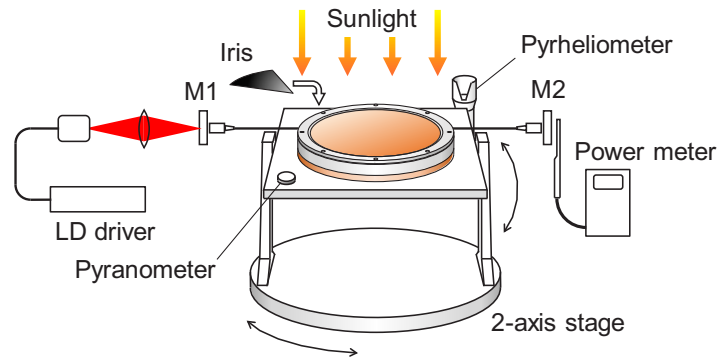
Fig. 5. Schematic drawing of the laser oscillation experiment setup.

from the front of the disk, and the laser output was measured with an optical power meter (ADC 82311B) placed at the M2 end.

The apparatus was rotated by a 2-axis manual stage such that it always faced the sun. Adjustments were made immediately before the experiment, and the apparatus was fixed during the experiment (several minutes). Direct solar irradiance was measured with a pyrheliometer (EKO MS-57). It varied from day to day and ranged from 850 to 950 W/m^2. Moreover, the total irradiance, including the diffuse part of sunlight, was measured with a pyranometer (EKO ML-02) installed on the surface of the 2-axis stage (tracking the sun). It also varied from day to day, ranging from 900 to 1000 W/m^2. For both the small signal gain and laser oscillation experiments, a variable iris was installed to partially block the aperture and adjust the irradiated solar power.

In both experiments, the temperature of the fiber disk was kept between -40 °C and -45 °C by a copper cooling plate chilled by a dry ice-methanol refrigerant, which was attached to the bottom surface of the chamber (see Fig. 1).

The most prominent feature of the fully planar SPFL is that it does not require solar tracking. In fact, the power received by the device decreases by a factor cosθ, where θ is the angle between the sun and the DM normal, and is maintained over 90% within ±26 degrees. To confirm this, we performed the experiment shown in Fig. 6. A Xe lamp (Photoron HVC-SL) was suspended in the air, and the SPFL was placed 1 m below it. The irradiance of the Xe lamp is 440 W/m^2 at the center of the SPFL with an e-folding radius of 14 cm. The SPFL can be tilted to any angle around its centerline. The differential gain was measured in the same way as in the outdoor experiment.
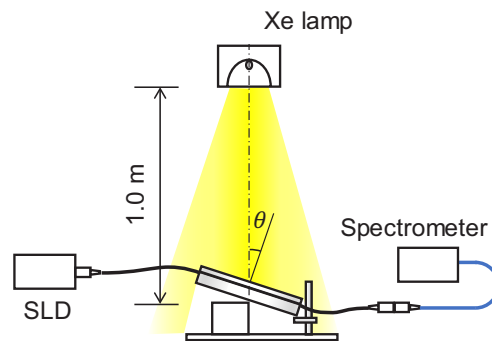

Fig. 6. Setup for irradiation angle insensitivity test.

3. Experimental results

3.1. Small-signal gain measurement

Figure 7 shows the results of the small-signal gain measurements. The horizontal axis is the direct solar power incident on the DM, and the vertical axis is the one-way differential gain. The active fiber used in this study has a broadband gain in the range of 1050 to 1130 nm, with a peak near 1064 nm [25]. The vertical axis of the graph represents $\ln(G) = \gamma_0 l$ at 1064 nm, where γ_0 is the small signal gain coefficient and l is the fiber length. The red circle plots show the results for the 105 m-long fiber, and blue square plots show the results for the 290 m-long fiber.
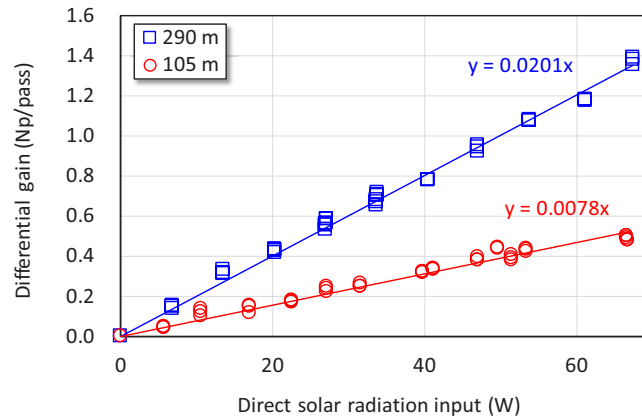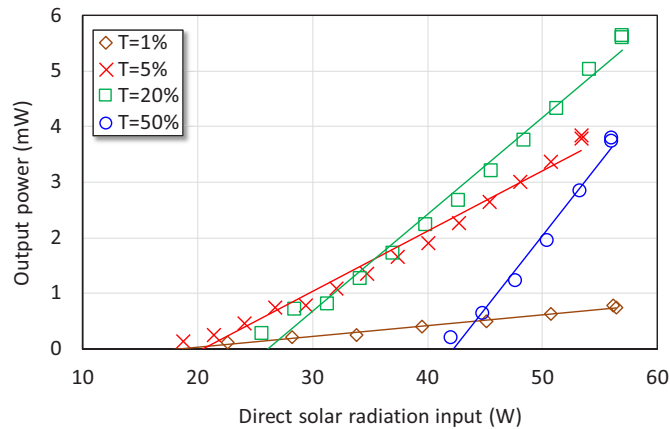

Fig. 7. One-way gain as a function of the direct solar radiation input for two different fiber lengths (105 m and 290 m).

The gain is proportional to the incident power and to the fiber length. The small signal gain coefficient γ_0 is proportional to the pump power density, i.e., the photon density confined by the LSC. As the fiber length increases, gain saturation will be observed because optical absorption by the fiber reduces the photon density. However, there is no evidence for this in Fig. 7 because the fiber length used in this study is not sufficient for saturation; our calculations indicate that the ideal fiber length for maximum laser power in a 30 cm disk is approximately 3 km [24]. The maximum gain achieved with the 290 m-long fiber was 1.4 Np/pass (4.1×).

### 3.2. Laser oscillation experiment

Figure 8 shows the relationship between the direct solar input and the laser power that was observed on the 105 m-long fiber. Partial reflectors with 1, 5, 10, 20, 30, and 50% transmittance were used. The results for 1, 5, 20, and 50% are shown. The relationship between pump power and output power was close to a linear function. However, the slope tended to be small near the oscillation threshold. This is because the fiber laser in this study oscillated in many longitudinal modes simultaneously due to spatial hole burning [28], and only some of them started to oscillate near the threshold. It is also possible that the transverse modes become more populated as the output power increases near the threshold, which also affects the slope efficiency. This phenomenon has also been observed in other broadband fiber lasers [29,30].

For each mirror transmittance, the relationship between pump power and laser power was approximated as a linear function near the oscillation threshold, and the oscillation threshold was determined from the intersection with the *x*-axis. The oscillation threshold at 1% mirror reflectance was 17 W. This was only 24% of typical natural sunlight and a significant improvement over a previous study [20].

Fig. 8. Laser output power as a function of the direct solar radiation input for the 105-m long fiber. The mirror transmittance is varied as a parameter.

The graph in Fig. 9 plots the mirror transmittance on the horizontal axis and the oscillation threshold power on the vertical axis. As expected, the relationship was linear. Extrapolating the mirror transmittance to zero, the oscillation threshold power at zero transmittance was 15 W. Applying this to Fig. 7, the laser oscillation threshold gain for this condition (0.117 Np/pass) was 0.51 dB/pass. Subtracting the loss of the pigtail mirror from this value, 0.44 dB/pass was the value at which the gain generated in the fiber was balanced by the intrinsic loss of the fiber. This corresponded to 4.2 dB/km, which was between the manufacturer's nominal value of 3 dB/km [20] and the measured value in our previous study of 5.4 dB/km ($1.25\,\mathrm{km}^{-1}$) [21].
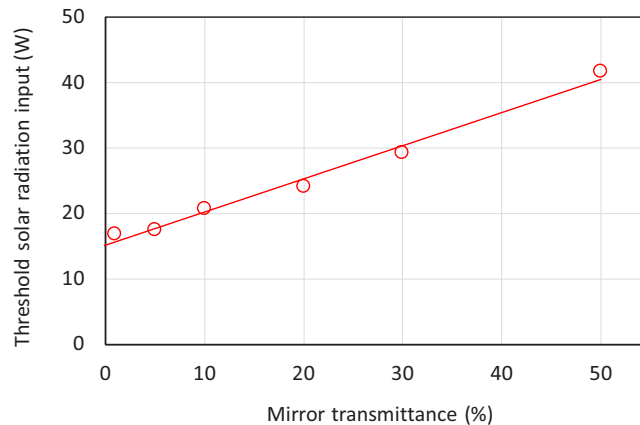
Fig. 9. Oscillation threshold power (direct sunlight) as a function of the output coupler transmittance.

Figure 10 shows a plot of mirror transmittance on the horizontal axis and laser power on the vertical axis for the 105 m-long and 290 m-long fibers. For the 290 m-long fiber, the reliability of the data was low, except for the highest powers at $T = 20\%$ and $T = 50\%$, because the fiber in the disk was broken after a few oscillation runs. Even though the fiber was broken, it was held in place with adhesive; thus, it did not become completely disconnected, and laser oscillation was assumed to occur. The maximum laser power at the 290 m-long fiber was 15 mW, more than 10 times the maximum of liquid LSC [20]. The optical-to-optical conversion efficiency was 0.023%, and the collection efficiency was 0.21 W/m^2.
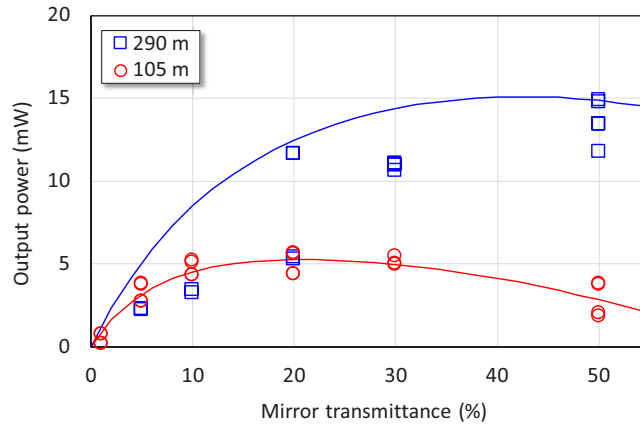
Fig. 10. Laser output power as a function of the mirror transmittance for two different fiber lengths (105 m and 290 m). Plots: experimental, lines: Rigrod fit.

3.3. Irradiation angle insensitivity test

Figure 11 shows the results of the test confirming the insensitivity of the gain to the angle of incidence. The horizontal axis is the angle between the Xe lamp and the SPFL normal, and the vertical axis is the normalized differential small-signal gain coefficient. The red circles represent the experimental results, and the blue line represents $\cos\theta$. The graph shows that the angular dependence of the small signal gain is well approximated by $\cos\theta$, as expected.
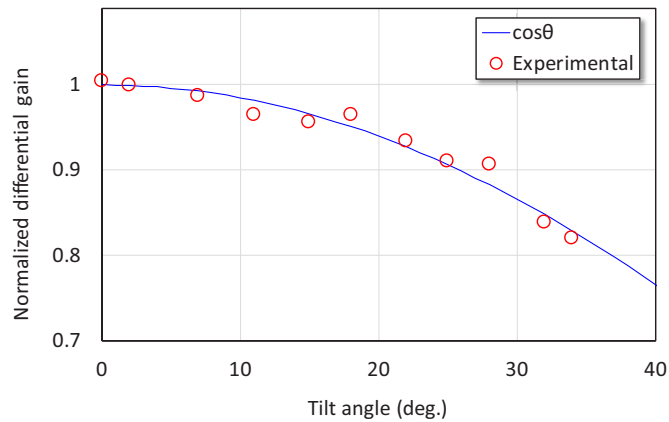
Fig. 11. Normalized differential gain coefficient as a function of the tilt angle.

4. Discussion

4.1. Rigrod analysis

The Rigrod equation [31] describes the laser power with a homogeneously broadened laser medium as a function of the mirror transmittance, as follows:

$$P = \frac{\gamma_0 l + \ln \sqrt{R_1 R_2}}{\left(1 + \sqrt{R_2/R_1}\right)\left(1 - \sqrt{R_1 R_2}\right)} I_s A T, \tag{2}$$

where $R_1 = 1 - a - a_M$ is the reflectivity of M1, $R_2 = 1 - a - a_M - T$ is the reflectivity of M2, a is the scattering loss of the resonator mirror, T is the transmittance of M2, γ_0 and I_s are the small signal gain coefficient and the saturation intensity of the medium, respectively, and l and A are the length and cross-sectional area of the medium, respectively [32]. $a_M = 1 - e^{-\alpha l}$ and represents the nonsaturable losses in the laser medium as the mirror losses, where α is the loss coefficient. This approximation is correct when $\gamma_0 >> \alpha$ [33]. In our previous study (laser oscillation by liquid LSC) [20], this approximation did not hold, and the exact solution was computed numerically. In this study, however, the approximate solution is used because it was confirmed that there is little difference between the two.

Using γ_0, I_s, and α as parameters, the best fit of the experimental results for the 105 m-long fiber was determined. The results were $\gamma_0 l = 0.62$ Np, $I_s = 8.5$ kW/cm^2, and $\alpha = 1.4$ dB/km. Compared to the experimental values, $\gamma_0 l$ is larger (Fig. 7), and α is smaller (4.2 dB/km). The reason for this is currently unknown. The possibility of inhomogeneous broadening of the medium was investigated [33], but the result was negative.

The red curve in Fig. 10 shows the calculated laser power for the 105 m-long fiber as a function of the mirror transmittance using the optimal parameter set. The Rigrod model is a good representation of the laser power dependence on the mirror transmittance.

We now have a model that predicts the output power of the SPL with a solid-state LSC for any given fiber length, input solar irradiance, and resonator coupling. Using this model, the calculated laser power for the 290 m-long fiber is shown in Fig. 10 with a blue curve. The highest laser powers observed at 20% and 50% transmittance are well represented by the Rigrod model.

The model was then used to calculate the relationship between incident solar power and laser power for the combination of the 290 m-long fiber and the $T = 50\%$ mirror. As a result, the calculated laser oscillation threshold pump power was 22 W, and the slope efficiency was 0.031%.

4.2. Investigation of the fiber breakage

The disk with the broken fiber was unmounted from the housing, the location of the broken fiber was confirmed, and the cause of the break was investigated. Figure 12 shows a photograph of the broken fiber disk.

One fiber crosses over another fiber in an X-shape and protrudes over the other fiber. During the experiment, the distance between DM and HR narrowed due to thermal contraction, causing the upper fiber to be subjected to bending stress, while the lower fiber became the fulcrum, leading to breakage.
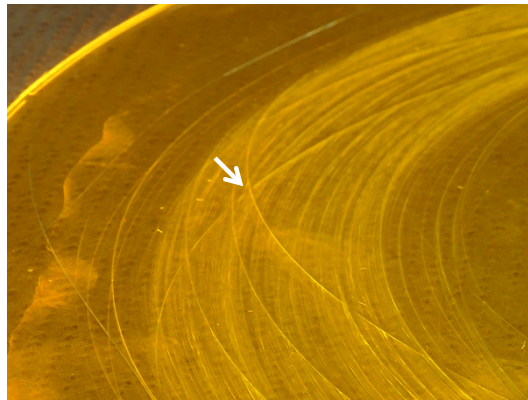
Fig. 12. Photograph of the disk with 290 m-long fiber. The arrow indicates the point of breakage.

The reason for this fiber arrangement is that the process of removing the protective resin was not optimized, and the fiber bundle loosened during the process. The fiber bundles were reassembled by hand, but crossings were inevitable, as shown in the photo. Another reason was that we tried to make the distance between the DM and HR as small as possible and did not take thermal shrinkage into account. All these problems are technical and easily avoidable and should be taken as lessons for future experiments.

4.3. Comparison with numerical calculations

We confirmed the effectiveness of solid-state LSCs via numerical calculations and published the results [24]. The laser power of a 30 cm diameter LSC with 190 m fiber length was predicted to increase from 1.3 mW for the liquid LSC to a maximum of 39 mW. Now, this result could be compared with the experimental results.

In the numerical calculations, the 190 m-long fiber was assumed to be embedded in a disk of dye-impregnated PMMA. In the present study, however, the fiber was attached to the substrate, which increased the overall thickness of the LSC, and the distance between the DM and the HRM increased from 1.5 mm to 2.5 mm. Moreover, the fiber length was 1.5 times longer than the calculation condition. In the first-order approximation, the expected output power was inversely proportional to the DM-HR distance and proportional to the fiber length. Thus, the experimental results were directly comparable to the numerical calculation with a mirror distance of 1.5 mm and a fiber length of 190 m.

Consequently, the laser power obtained in the experiment was lower than that calculated. We speculated that this was because the fiber was attached to the quartz substrate. This created an uneven surface on the LSC and prevented total internal reflection. In Ref. [24], we predicted that the laser power of Design 1, in which the fiber was placed outside the disk, was 17 mW, and the experimental results were similar to this value. Based on the above results, the effectiveness of our proposed method was experimentally confirmed.

4.4. Possibility of room-temperature operation

The reason our lasers can oscillate at the intensity of natural sunlight is simply because we employ a "small gain compensated by large gain length" strategy. Thus, even small losses in the fiber are large enough to prevent the laser from oscillating. The most obvious example of this is the population of the lower laser level at room temperature. The measured losses of our fiber at 1060 nm are 30 dB/km at room temperature [21], but cooling reduces this to 3 to 5 dB/km (Section 3.2). The differential gain coefficient obtained in this study is 1.4 Np/290 m = 21 dB/km, indicating that cooling is essential. On the other hand, in a previous study [24], the small-signal gain coefficient of Design 2 reached 65 dB/km, indicating that laser oscillation is possible at room temperature. The laser output power was calculated to be one-fifth of the cooled condition.

Thus, in principle, the proposed method enables laser oscillation at room temperature, but the output power will always be lower than that of the cooled condition. To reduce the difference, the gain factor of the fiber must be improved, and the most effective means are to increase the photon absorption efficiency and the photon confinement efficiency. The former can be improved by applying quantum dots that fluoresce in the near infrared region, and the latter can be done directly by improving the design of the dielectric multilayer mirrors and reducing the radiation loss from the side reflector.

4.5. Comparison with other solar-pumped fiber lasers

Fiber as a laser medium is characterized by its extremely high cross-sectional area/length ratio and bending flexibility compared to other forms of laser media. Our idea is one of the applications that exploits this feature, but other ideas for solar pumped lasers that exploit the fiber gain medium have been presented. Guo *et al*. proposed SPFLs in which the fiber is wound in a cylindrical

shape and pumped laterally by focusing sunlight in a ring shape [34] or pumped from the side of the cylinder [35]. The advantage is the better coupling of sunlight with the gain medium due to the large interaction cross section.

Mizuno *et al.* have taken a different approach to SPFL that exploits the properties of the fiber medium [36]. Their SPFL is end-pumped, so the solar concentration required for their SPFL is not much different from other SPLs, but the large surface area of the fiber medium allowed them to operate continuously with natural air convection cooling. The problem of inherent difficulty in scaling up is solved by arranging many lasers [37].

On the other hand, it is undeniable that the high barriers to entry in this field have hindered SPFL research, as it is currently very difficult to obtain special fibers suitable for solar-pumped lasers. We hope that the fiber laser research community and industry will be interested in this area of research.

5. Conclusions

We investigated a fully planar solar pumped fiber laser (SPFL) without any focusing device, such as a lens or mirror. To achieve this goal, we developed a confinement mechanism that combined a fluorescent sensitizer with a chamber consisting of a dichroic mirror (DM) and a highly reflective mirror (HRM) to efficiently couple solar photons into an optical fiber. In the past, dye molecules dissolved in a liquid were used as sensitizers. However, in that case, high reflectivity could not be achieved due to the direct contact of DM and HRM with the liquid sensitizer. In our study, a solid-state luminescent solar collector (LSC) was achieved by impregnating the sensitizer into a resin and coating it on a quartz substrate. Although solid-state LSCs were not usually combined with DM or HRM, a previous study showed that the use of DM and HRM increased the photon density by more than a factor of two compared to the total internal reflection alone. This was an immense advantage of our concept, which was characterized by extremely low gain per unit length.

A fully planar SPFL with a solid-state LSC was fabricated with the same aperture as that of the liquid sensitizer. LSC disks with a 105 m-long fiber and a 290 m-long fiber were fabricated, and the small signal gain and laser power were measured for both disks under the illumination of natural sunlight. The laser with a 105 m-long fiber had a one-way gain of 0.5 Np (65%/pass) and a maximum output power of 5.6 mW. Experiments with different sunlight intensities showed that the laser oscillation threshold was 24% of natural sunlight, which was significantly lower than that in a previous study (60%). However, the laser with a fiber length of 290 m did not provide sufficient data because the fiber broke inside the disk during the first set of experiments. Nevertheless, a one-way gain of 1.4 Np (310%/pass) and a maximum output power of 15 mW were obtained. It had a 12-fold larger output power than the liquid LSC and corresponded to an optical-to-optical conversion efficiency of 0.023% and a collection efficiency of 0.21 W/m^2.

A Rigrod model was constructed from the results of laser oscillation experiments on the 105 m-long fiber to predict the performance of the 290 m-long fiber. The results were in good agreement with the limited experimental results. Although it was not possible to obtain the slope efficiency for the 290 m-long fiber, it was estimated to be 0.031% from the Rigrod model.

The results of this study show that the fully planar SPFL can achieve the theoretically calculated laser output power. Under ideal conditions, the optical-to-optical conversion efficiency of the fully planar SPFL has been calculated to reach 8% [20]. Since the efficiency of wavelength conversion and the efficiency of photocatalytic hydrogen generation by UV light are theoretically close to 100%, the combination of a solar-pumped laser and photocatalytic hydrogen generation is potentially superior to other methods of hydrogen generation. In addition, the fully planar SPL can be easily configured into a large-scale system through parallelization [38]. We are developing basic technologies for higher efficiency, wavelength conversion, and scaling-up with catalytic hydrogen generation in mind.

Disclosures. The authors declare no conflicts of interest.

Data availability. Data underlying the results presented in this paper are not publicly available at this time but may be obtained from the authors upon reasonable request.

References

1. D. Graham-Rowe, "Solar-powered lasers," Nat. Photonics **4**(2), 64–65 (2010).
2. D. Liang, J. Almeida, C. Vistas, B. Tibúrcio, and D. Garcia, *Solar-Pumped Lasers–With Examples of Numerical Analysis of Solid-State Lasers* (Springer, 2023).
3. S. Berwal, N. Khatri, and D. Kim, "A review on design modalities of solar-pumped solid-state laser," Applied Surface Science Advances **12**, 100348 (2022).
4. D. Liang, J. Almeida, C. R. Vistas, and E. Guillot, "Solar-pumped Nd:YAG laser with 31.5 W/m^2 multimode and 7.9 W/m^2 TEM$_{00}$-mode collection efficiencies," Sol. Energy Mater. Sol. Cells **159**, 435–439 (2017).
5. D. Liang, C. R. Vistas, D. Garcia, B. D. Tibúrcio, M. Catela, H. Costa, E. Guillot, and J. Almeida, "Most efficient simultaneous solar laser emissions from three Ce:Nd:YAG rods within a single pump cavity," Sol. Energy Mater. Sol. Cells **246**, 111921 (2022).
6. T. Motohiro and K. Hasegawa, "Assessment of possible performances of compact solar-pumped lasers using transparent Cr3$^+$, Nd3$^+$-co-doped YAG ceramics micro rods," Optik **284**, 170942 (2023).
7. Z. Cai, C. Zhao, Z. Zhao, J. Zhang, Z. Zhang, and H. Zhang, "Efficient 38.8 W/m^2 solar pumped laser with a Ce:Nd:YAG crystal and a Fresnel lens," Opt. Express **31**(2), 1340–1353 (2023).
8. T. Yabe, S. Uchida, K. Ikuta, K. Yoshida, C. Baasandash, M. S. Mohamed, Y. Sakurai, Y. Ogata, M. Tuji, Y. Mori, Y. Satoh, T. Ohkubo, M. Murahara, A. Ikesue, M. Nakatsuka, T. Saiki, S. Motokoshi, and C. Yamanaka, "Demonstrated fossil-fuel-free energy cycle using magnesium and laser," Appl. Phys. Lett. **89**(26), 261107 (2006).
9. Y. Takeda, H. Iizuka, S. Mizuno, K. Hasegawa, T. Ichikawa, H. Ito, T. Kajino, A. Ichiki, and T. Motohiro, "Silicon photovoltaic cells coupled with solar-pumped fiber lasers emitting at 1064 nm," J. Appl. Phys. **116**(1), 014501 (2014).
10. T. Motohiro, Y. Takeda, H. Ito, K. Hasegawa, A. Ikesue, T. Ichikawa, K. Higuchi, A. Ichiki, S. Mizuno, T. Ito, N. Yamada, H. N. Luitel, T. Kajino, H. Terazawa, S. Takimoto, and K. Watanabe, "Concept of the solar-pumped laser-photovoltaics combined system and its application to laser beam power feeding to electric vehicles," Jpn. J. Appl. Phys. **56**(8S2), 08MA07 (2017).
11. T. Hisatomi and K. Domen, "Reaction systems for solar hydrogen production via water splitting with particulate semiconductor photocatalysts," Nat. Catal. **2**(5), 387–399 (2019).
12. T. Takata, J. Jiang, Y. Sakata, M. Nakabayashi, N. Shibata, V. Nandal, K. Seki, T. Hisatomi, and K. Domen, "Photocatalytic water splitting with a quantum efficiency of almost unity," Nature **581**(7809), 411–414 (2020).
13. Y. K. Bae, "Prospective of Photon Propulsion for Interstellar Flight," Phys. Procedia **38**, 253–279 (2012).
14. D. Goto, H. Yoshida, H. Suzuki, K. Kisara, and K. Ohashi, "The Overview of JAXA Laser Energy Transmission R&D Activities and the Orbital Experiments Concept on ISS-JEM," *Proc. International Conference on Space Optical Systems and Applications*, S5–2 (2014).
15. Y. A. Abdel-Hadi, "Space-based solar laser system simulation to transfer power onto the earth," NRIAG Journal of Astronomy and Geophysics **9**(1), 558–562 (2020).
16. R. J. De Young, G. D. Walberg, E. J. Conway, and L. W. Jones, "A NASA high-power space-based laser research and applications program," NASA SP **464**, 19830018929 (1983).
17. Z. Guan, C. M. Zhao, S. H. Yang, Y. Wang, J. Y. Ke, and H. Y. Zhang, "Demonstration of a free-space optical communication system using a solar-pumped laser as signal transmitter," Laser Phys. Lett. **14**(5), 055804 (2017).
18. S. Mehellou, F. Rehouma, N. Hamrouni, and L. Bouras, "Thermal loading effects on Nd:YAG solar-laser performance in end-pumping and side-pumping configurations: a review," Opt. Eng. **57**(12), 1 (2018).
19. B. D. Tibúrcio, D. Liang, J. Almeida, D. Garcia, M. Catela, H. Costa, and C. R. Vistas, "Tracking error compensation capacity measurement of a dual-rod side-pumping solar laser," Renewable Energy **195**, 1253–1261 (2022).
20. T. Masuda, M. Iyoda, Y. Yasumatsu, S. Dottermusch, I. A. Howard, B. S. Richards, J.-F. Bisson, and M. Endo, "A fully planar solar pumped laser based on a luminescent solar collector," Commun. Phys. **3**(1), 60 (2020).
21. J.-F. Bisson, M. Iyoda, Y. Yasumatsu, M. Endo, and T. Masuda, "Effect of the thermally excited lower laser level in a neodymium-doped fiber," J. Opt. Soc. Am. B **36**(3), 736 (2019).
22. M. Endo, J.-F. Bisson, and T. Masuda, "Monte Carlo simulation of a transversely excited solar-pumped fiber laser," Jpn. J. Appl. Phys. **58**(11), 112006 (2019).
23. T. Masuda, Y. Zhang, C. Ding, F. Liu, K. Sasaki, Q. Shen, and M. Endo, "All-inorganic cesium lead halide perovskite nanocrystals for solar-pumped laser application," J. Appl. Phys. **127**(24), 243104 (2020).
24. S. Dottermusch, T. Masuda, M. Endo, B. S. Richards, and I. A. Howard, "Solar Pumping of Fiber Lasers with Solid–State Luminescent Concentrators: Design Optimization by Ray Tracing," Adv. Opt. Mater. **9**(12), 2100479 (2021).

25. T. Masuda, K. Aoyagi, S. Dottermusch, I. A. Howard, B. S. Richards, and M. Endo, "Light Management for Enhancing Optical Gain in a Solar–Pumped Fiber Laser Employing a Solid–State Luminescent Solar Concentrator," Adv. Photonics Res. **3**(2), 2100214 (2022).

26. M. Carrascosa, S. Unamuno, and F. Agullo-Lopez, "Monte Carlo simulation of the performance of PMMA luminescent solar collectors," Appl. Opt. **22**(20), 3236 (1983).

27. T. Masuda, M. Iyoda, Y. Yasumatsu, and M. Endo, "Low-loss pigtail reflector for fiber lasers," Rev. Sci. Instrum. **88**(5), 053112 (2017).

28. R. Paschotta, J. Nilsson, L. Reekie, A. C. Trooper, and D. C. Hanna, "Single-frequency ytterbium-doped fiber laser stabilized by spatial hole burning," Opt. Lett. **22**(1), 40–42 (1997).

29. J. Mrazek, I. Kasik, L. Prochazkova, V. Cuba, J. Aubrecht, J. Cajzl, O. Podrazky, P. Peterka, and M. Nikl, "Active Optical Fibers Doped with Ceramic Nanocrystals," AEEE **12**(6), 567–574 (2015).

30. M. Kochanowicz, J. Zmojda, P. Miluski, A. Baranowska, M. Leich, A. Schwuchow, M. Jäger, M. Kuwik, J. Pisarska, W. A. Pisarski, and D. Dorosz, "Tm^{3+}/Ho^{3+} co-doped germanate glass and double-clad optical fiber for broadband emission and lasing above 2 µm," Opt. Mater. Express **9**(3), 1450–1457 (2019).

31. W. W. Rigrod, "Saturation Effects in High–Gain Lasers," J. Appl. Phys. **36**(8), 2487–2490 (1965).

32. A. E. Siegman, *Lasers* (University Science Books 1986), pp. 485–487.

33. D. L. Carroll, "Effects of a nonhomogeneous gain saturation law on predicted performance of a high-gain and a low-gain laser systems," Appl. Opt. **33**(9), 1673–1681 (1994).

34. P. Guo, M. Ou, Y. Liu, Y. Tang, J. Zhou, and L. Lan, "Transversely pumped solar Nd^{3+}-doped fiber laser," Optik **247**, 167933 (2021).

35. P. Guo, J. Zhang, Z. Chen, L. Lan, Y. Liu, Y. Tang, and X. Ma, "Side-pumped solar Nd-doped fiber laser based on off-axis parabolic mirror array," Optik **271**, 170096 (2022).

36. S. Mizuno, H. Ito, K. Hasegawa, T. Suzuki, and Y. Ohishi, "Laser emission from a solar-pumped fiber," Opt. Express **20**(6), 5891–5895 (2012).

37. T. Motohiro, A. Ichiki, T. Ichikawa, H. Ito, K. Hasegawa, S. Mizuno, T. Ito, T. Kajino, Y. Takeda, and K. Higuchi, "Consideration of coordinated solar tracking of an array of compact solar-pumped lasers combined with photovoltaic cells for electricity generation," Jpn. J. Appl. Phys. **54**(8S1), 08KE04 (2015).

38. Cover Image, Advanced Optical Materials, Vol. 9, No. 12, June 18 (2021).